Special Issue

Applied Spectroscopy

Confocal Raman Microscopy for Measuring In Situ Temperature-Dependent Structural Changes in Poly(Ethylene Oxide) Thin Films

Applied Spectroscopy
1–12

DOI: 10.1177/00037028241310904
journals.sagepub.com/home/asp
Sage

Miharu Koh[1], Jay P. Kitt[1], Andrew D. Pendergast[1], Joel M. Harris[1], Shelley D. Minteer[1,2], and Carol Korzeniewski[1,3]

Abstract

Crystallization from the melt is a critical process governing the properties of semi-crystalline polymeric materials. While structural analyses of melting and crystallization transitions in bulk polymers have been widely reported, in contrast, those in thin polymer films on solid supports have been underexplored. Herein, in situ Raman microscopy and self-modeling curve resolution (SMCR) analysis are applied to investigate the temperature-dependent structural changes in poly(ethylene oxide) (PEO) films during melting and crystallization phase transitions. By resolving complex overlapping sets of spectra, SMCR analysis reveals that the thermal transitions of 50 µm thick PEO films comprise two structural phases: an ordered crystalline phase and a disordered amorphous phase. The ordered structure of the crystalline PEO film entirely disappears as the polymer is heated; conversely, the disordered structure of the amorphous PEO film reverts to the ordered structure as the polymer is cooled. Broadening of the Raman bands was observed in PEO films above the melting temperature (67 °C), while sharpening of bands was observed below the crystallization temperature (45 °C). The temperatures at which these spectral changes occurred were in good agreement with differential scanning calorimetry (DSC) measurements, especially during the melting transition. The results illustrate that in situ Raman microscopy coupled with SMCR analysis is a powerful approach for unraveling complex structural changes in thin polymer films during melting and crystallization processes. Furthermore, we show that confocal Raman microscopy opens opportunities to apply the methodology to interrogate the structural features of PEO or other surface-supported polymer films as thin as 2 µm, a thickness regime beyond the reach of conventional thermal analysis techniques.

Keywords

Confocal Raman microscopy, poly(ethylene oxide) thin films, PEO thin films, polymer phase transitions, self-modeling curve resolution, confocal Raman depth profiling

Date received: 15 November 2024; accepted: 9 December 2024

Introduction

A fundamental understanding of structural and conformational changes during melting and crystallization of semi-crystalline polymeric systems is crucial for controlling their mechanical properties, including tensile strength, rigidity, and durability.[1] Microstructures and superstructures formed in the crystalline polymeric solid during cooling from the molten phase strongly influence these properties.[1–3] Many techniques have been used to investigate polymer phase transitions, including differential scanning calorimetry (DSC),[4] X-ray diffraction[5–7] and reflectivity,[8] neutron scattering,[9,10] nuclear magnetic resonance (NMR),[11,12] Raman spectroscopy,[13–20] infrared (IR) spectroscopy,[17–19] and molecular dynamics simulations.[21] Despite the variety of methods employed to study polymer phase transitions, limitations exist with these techniques. Calorimetry, while providing a

[1]Department of Chemistry, University of Utah, Salt Lake City, Utah, USA
[2]Department of Chemistry, Missouri University of Science and Technology, Rolla, MO, USA
[3]Department of Chemistry and Biochemistry, Texas Tech University, Lubbock, Texas, USA

Corresponding Authors:
Shelley D. Minteer, Department of Chemistry, University of Utah, Salt Lake City, Utah 84112, USA. Department of Chemistry, Missouri University of Science and Technology, Rolla, Missouri, USA
Email: shelley.minteer@mst.edu

Carol Korzeniewski, Department of Chemistry, University of Utah, Salt Lake City, Utah 84112, USA. Department of Chemistry and Biochemistry, Texas Tech University, Lubbock, Texas 79409, USA.
Email: carol.korzeniewski@ttu.edu

wealth of thermodynamic data (i.e., transition temperatures, heat capacity, and enthalpy values), lacks molecular-level structural information about the polymer transformation. While such information is obtainable from other techniques, most require large sample volumes, making micrometer-scale investigations of thin films of polymeric materials difficult.

Thin polymeric films have been widely studied and employed in many applications, including coatings,[22] optoelectronics,[23,24] and energy-harvesting/storage devices.[25–27] These advances highlight the need for methods to interrogate the structure–function relationships of thin polymer films with thicknesses ranging from a few nanometers to several micrometers.[8] Current methods for investigating such films are X-ray diffraction and neutron scattering, both of which provide fine structural detail. These techniques, however, can be costly and require expertise in sample preparation and instrument operation. Furthermore, neutron scattering has limited availability. In contrast, vibrational spectroscopy is a low-cost, readily accessible methodology that uses low-energy photons to provide insights into polymer structure and conformation at the molecular level. Recently, Raman spectroscopy was applied to measure the thermal properties of a bulk polymer sample, where structural changes occurring during melting and crystallization of isotactic poly(propylene) were investigated.[13] Although Raman spectroscopy is well-suited to the analysis of bulk polymers, the large probe volumes and modest collection efficiency of traditional Raman scattering measurements limit their application in the study of thin polymer films.

For this work, we employed a confocal Raman microscope[28–31] to measure within a small (~3 μm^3)[32] spatial region inside a thin polymer film and investigate structural changes during polymer melting and recrystallization. Spectral monitoring of the phase transitions was achieved by carefully positioning the microscope confocal probe volume[30–35] within the sample. After focusing the excitation radiation inside the polymer and collecting backscattered Raman light through the same objective, the confocal probe volume was defined by spatially filtering the scattered radiation through a well-defined aperture to limit collection to a small volume within the focal region.[29,30,32,34,36–38] The spatial selectivity and potential for high collection efficiency of confocal Raman microscopy have made the measurement technique a practical approach for investigating the chemistry of small polymeric particles[33,39] and processes within individual phospholipid vesicles[40,41] and thin redox-polymer[31] films. These studies have employed high numerical-aperture oil-immersion objectives, which provide outstanding collection efficiency and spatial resolution. Despite these advantages, oil objectives are not well-suited to confocal Raman microscopy studies of thermal phase transitions in polymer thin films. The immersion oil conducts heat from the sample, leading to significant temperature errors. In the reported work, we therefore employed a long-working-distance air objective that allows an air gap between the lens and sample to minimize heat loss from the sample. While air objectives compromise both collection efficiency and spatial resolution in confocal Raman microscopy,[28,29,42] we show that by trading off depth resolution for increased sensitivity and thermal stability, an air objective can be effectively deployed to investigate melting phase transitions within thin polymer samples.

For the purpose of developing this methodology, poly(ethylene oxide) (PEO), a well-studied polymer with broad applications, was chosen. PEO consists of repeating units of hydrophobic ethylene groups ($–CH_2–CH_2–$) and ether linkages (–O–) (Scheme 1). The presence of weakly hydrophilic oxygen makes PEO a versatile semi-crystalline polymer with a wide range of applications, including drug delivery systems,[43] polymer electrolytes,[44] and biosensors.[45] Early studies characterized the crystallinity properties of PEO.[5–7] X-ray and vibrational spectroscopy measurements revealed that in the crystalline form, PEO oligomers adopt a 7_2 helical structure with a period of 19.3 Å and a succession of trans (COCC), gauche (OCCO), and trans (CCOC) conformations along the chain axis.[5,17] When the temperature of crystalline PEO is raised above its melting transition, rotations about the C–O and C–C bonds cause distortion of the helical structure.[16,46] In some studies, vibrational modes have been assigned to the development of trans conformations about the C–C bonds (or OCCO dihedral angle) during PEO melting.[15,18,19] However, recent findings suggest that C–O bond rotation is the driver for PEO melting, enabling the trans C–O bonds in the crystalline state to transition to a gauche conformation in the molten state while the gauche C–C bonds remain unchanged.[47,48] Although PEO has been extensively investigated, few studies have probed the structural changes in situ during heating and cooling, especially for higher molecular weight polymers (e.g., $M_w = 200\,000$ g/mol). Furthermore, to the authors' knowledge, no thermal phase transition studies of PEO thin films have been reported.

This work investigates how confocal Raman microscopy can be applied to monitor the structural evolution of PEO thin films in situ during melting and recrystallization. Self-modeling curve resolution (SMCR) analysis[49–51] is utilized to examine the temperature-dependent spectra, allowing resolution of overlapped spectral modes that evolve as melting or crystallization occurs. SMCR reveals that the structure of PEO during melting and recrystallization can be represented by two spectral components, one associated with a crystalline phase and the other with an amorphous phase, and predicts the corresponding melting/crystallization profiles for each. The spectral changes associated with PEO melting and recrystallization are considered in detail, along

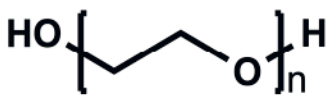

Scheme 1. The chemical structure of poly(ethylene oxide) (PEO).

with the control and characteristics of the confocal probe volume produced by an air-objective in confocal Raman microscopy of polymer thin films.

Experimental

Materials and Methods

Reagents and Materials. Poly(ethylene oxide) powder (M_w = 200 000) was purchased (Sigma Aldrich, USA). Acetonitrile (HPLC Grade) was obtained (Fischer Scientific, USA). Microscope coverslips (No. 1.5 thickness, BK-7 glass) were obtained (Electron Microscopy Sciences, USA). The proportional–integral–derivative (PID) controller (Model P48-E, 1/16 DIN process controller) was obtained (Red Lion, USA). The heating block (Filfeel, 110 V, 140 W) was obtained (Amazon.com). Single-layer graphene (SLG) was purchased, (ACS Material, USA).

Sample Preparation and Characterization. PEO thin films for in situ confocal Raman microscopy study were prepared by drop-casting material dissolved in acetonitrile (50 mg/mL) onto a microscope coverslip (No. 1.5 thickness, BK-7 glass) followed by annealing in a 70 °C oven for 30 min. The films were then adhered to a copper block for direct contact and efficient heat transfer (see below, Figure 1, and related text). The PEO film thicknesses (~50 μm) were estimated from the mass of the deposited polymer (50 mg), the area of the dried sample (~4 cm^2), and the density of PEO (1.21 g/cm^3, as specified by the supplier). For thinner PEO film (~2 μm), the dip-coating technique was employed, and scanning electron microscopy (SEM) was used to confirm the film thickness (Figure S1, Supplemental Material).

Confocal Raman Microscopy. The confocal Raman microscope system was adapted from previously reported work.[30,36] Briefly, sample excitation was provided by a diode-pumped solid-state laser operating at 660 nm (Gem 660, Laser Quantum, USA) with an output power of 200 mW, which was passed through a narrowband laser line filter (Semrock) to exclude any light from the exciting diodes. The laser beam was expanded (10×, Thorlabs, USA) and was directed into the rear port of a Nikon Eclipse TE 200 inverted microscope (Nikon, USA). The beam was then reflected by a dichroic mirror (Semrock) to slightly overfill the rear aperture of a 100×, 0.70 NA air objective (Nikon, L Plan EPI SLWD) and focused within the PEO film deposited on a microscope coverslip (no. 1.5 thickness, BK-7 glass). The scattered light from the sample was collected with the same objective and passed through the dichroic mirror and high-pass filter (Semrock). Raman scattered light was then focused onto the entrance slit of a grating monochromator (Shamrock 500i, Andor, UK). Raman spectra were obtained using a 300 lines/mm diffraction grating blazed at 760 nm. Raman scattered light was detected by a charge-coupled device (CCD) camera (iDus DU416A, Andor). The entrance slit of the monochromator was set to 50 μm, providing 7 cm^{-1} resolution. This slit width also defines the confocal aperture in the horizontal dimension, while the vertical dimension of the confocal aperture (165 μm radius) is defined by 22 rows of the CCD that are binned to collect intensity.[52] This asymmetric confocal aperture was designed to increase scattered-light collection efficiency from the 50 μm PEO films by trading off depth resolution, allowing scattering from greater distances from the focal plane to be detected. Based on this aperture size, the objective magnification, and numerical aperture (Figure S2, Supplemental Material),[30,53] the depth of field in the vertical dimension at 63% detection efficiency[29] (full width at 10% maximum) is 10.1 μm, which is sufficient resolution to sample the interior of a 50 μm film. Raman spectra were acquired at three-minute intervals with an integration period of 100 s.

Raman scattering from PEO films was collected by bringing the laser beam to a focus at the coverslip–polymer interface and centering the spot on the polymer film. For the 50 μm drop-cast films, the microscope objective was translated upward in the z-dimension to position the confocal probe volume ~20 μm above the coverslip–polymer interface, where the highest collection efficiency was observed.

Temperature-Controlled Confocal Raman Microscopy Setup. The cell was designed for the stage of the inverted Raman microscope. The inverted geometry was chosen to simplify control of the sample environment, including temperature and the surrounding dry N_2 atmosphere. The arrangement is depicted in Figure 1. A heating block controlled the temperature of a copper block that was in direct contact with the PEO film. The weight of the heater and copper block pressed the PEO film (~50 μm) against the glass microscope coverslip, allowing for good film contact with the glass and copper surfaces and providing even temperature distribution over the sample. The copper block (21 mm × 21 mm × 2.4 mm) was chosen for its high thermal conductivity. A hole was drilled at the side extending 1 cm into the block to accommodate the placement of the ~1 mm diameter thermocouple lead. The copper block was coupled to the heater with a

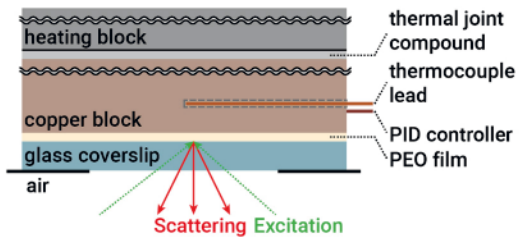

Figure 1. Schematic of the temperature-controlled confocal Raman microscopy setup. The wavy lines indicate sections of non-continuous scaling. During Raman experiments, the assembly was covered by a styrofoam enclosure that reduced thermal loss and allowed the sample to be kept in a dry N_2 environment.

silicone-based thermal compound (Wakefield Thermal, USA). Temperature was regulated with a PID controller (Red Lion Controls, USA). A styrofoam enclosure covered the assembly shown in Figure 1 to minimize thermal loss and maintain a dry N_2 atmosphere.

Temperature-controlled in situ Raman microscopy analysis was conducted while the sample temperature was varied at a heating and cooling rate of 1 °C/min. The temperature was ramped from 22 °C to 75 °C, held at 75 °C for 20 min, and ramped down to 30 °C in a dry nitrogen environment in the temperature-controlled Raman microscopy setup (Figure 1). Each spectrum recorded during the period was assigned the temperature measured at the mid-point of the 100 s spectral acquisition period. This mid-point temperature was determined from a linear fit of the logged temperature-time data measured at the thermocouple. Obtained slopes of 0.984 ± 0.002 °C/min and -0.990 ± 0.002 °C/min for heating and cooling, respectively, confirmed the 1 °C/min nominal rate set at the PID controller.

While an oil-immersion objective was incorporated into the initial design due to its high collection efficiency and depth resolution, the heat loss from the sample through the coverslip was substantial when in contact with the immersion oil. Thus, an air objective was chosen since air can serve as a thermal insulator, providing better control over the sample temperature. To test the thermal response of the cell design with an air objective, finite element modeling of temperature profiles in the cell and sample was conducted. As shown in the Supplemental Material (Figures S4–S6, Supplemental Material), the heat is distributed equally across the 50 µm PEO thin film at the same temperature as the copper block that houses the thermocouple; the temperature of the sample responds quickly to changes in the copper block, reaching the thermal equilibrium after two seconds. When a PEO film undergoes temperature-dependent phase transitions, the densities correspondingly change with temperature. Thus, the location of the focal volume is expected to change during in situ temperature-dependent studies. For this reason, the focus position was adjusted for maximum signal before each data collection to correct for the refractive index changes.

Differential Scanning Calorimetry (DSC). The DSC measurements were performed with a DSC 3500 Sirius differential scanning calorimeter (Netzsch, USA). The sample (10 mg) was packed and sealed in an aluminum crucible. The calorimeter cell was heated from 0 °C to 120 °C, maintained at 120 °C for 20 min, and cooled from 120 °C to 0 °C at a rate of 1 °C/min. All calorimetric measurements were conducted under a dry nitrogen atmosphere. The enthalpies of melting and crystallization transitions were baseline-corrected and normalized to their maximum values.

Multidimensional Data Analysis. Temperature-dependent Raman spectral datasets were analyzed by the model-free multivariate SMCR analysis method,[49–51] as applied previously to interpret temperature-dependent Raman spectra.[54–56] Custom scripts were executed in Matlab (version R2021b; MathWorks). Prior to analysis, the spectra were truncated to the frequency region of interest, baseline-corrected using a rolling-circle high-pass filter,[57] and normalized to the integrated spectral area.

The use of SMCR can resolve overlapping spectral changes and extract underlying component responses without requiring prior knowledge of a model of the process. The temperature-dependent Raman spectra were analyzed by SMCR analysis as follows. Baseline-corrected and normalized spectra acquired versus temperature are organized into a data matrix, D, of r rows and c columns. The rows denote the index on the Raman shift frequencies, and the columns correspond to the temperatures at which Raman spectra were measured. This matrix D can be expressed as the product of an $r \times i$ matrix (A) containing i pure component spectra and an $i \times c$ matrix (C) containing temperature-dependent concentration coefficients:

$$D = AC \tag{1}$$

The goal of SMCR analysis is to resolve D into its factor matrices A and C by an eigenvector decomposition. The first step is principal component analysis (PCA),[50] where the data are decomposed into a matrix of orthogonal eigenvectors (Q) and their respective scores (λ). The eigenvectors in Q represent the correlated changes in the scattering intensity in the temperature dimension, and the λ diagonal matrix containing eigenvalues corresponds to the relative magnitude of each eigenvector's contribution to the spectral data.

Several approaches have been developed to identify significant correlations in real datasets and eliminate the uncorrelated behavior due to noise. Fisher variance ratio or F-test on the scores and careful inspection of the eigenvector shapes for non-random variation are evaluated to identify the number of real components.[49–51] The Q matrix can then be truncated into a smaller matrix of principal components ($\hat{Q}$). This process removes the uncorrelated noise while preserving the correlated behavior of real components from the dataset.

The next step is to find the linear combinations of the eigenvectors that correspond to the real component responses in the data. The data matrix D is projected onto the composition eigenvectors, $\hat{Q}$, to produce a matrix of principal-component spectral eigenvectors (U):

$$U = D\hat{Q} \tag{2}$$

A transformation matrix (K) is postulated that rotates the abstract eigenvectors U and $\hat{Q}$ from eigenvector space into real space, generating component spectra $\hat{A}$ and temperature-dependent concentration vector $\hat{C}$, respectively.

$$\hat{A} = UK^{-1} \tag{3}$$

$$\hat{C} = K\hat{Q}^T \tag{4}$$

The search for K is guided by the correlated intensity variation in D, which is a linear combination of the pure component loadings in U, so that a plot of the loadings U in the space of $\hat{Q}^T$ is linear. For a two-component system, this produces a linear plot where the points at the extremes represent the wavenumbers at which 'purest' component behavior was measured. The search for K is confined along this line where the best coefficients are subject to the constraint that spectra $\hat{A}$ and component concentrations $\hat{\mathbf{C}}$ are not negative. The SMCR model data matrix ($\hat{D}$) is then represented by the product of $\hat{A}$ and $\hat{C}$:

$$\hat{D} = \hat{A}\hat{C} = UK^{-1}K\hat{Q}^T \quad (5)$$

The SMCR analysis presented here is used to resolve spectral changes occurring within PEO thin films during temperature-dependent melting and crystallization transitions. The entire dataset of temperature-dependent spectral changes in PEO thin films exhibits two significant components according to PCA. The fit quality of the model data matrix $\hat{D}$ to the experimental data D is shown in the Supplemental Material.

Finite Element Analysis. Heat transfer and the temperature profile within the PEO film were simulated using the finite element method within COMSOL Multiphysics (v.5.5) using the Heat Transfer in Solids (*ht*) module in two-dimensional geometry, as shown in Figures S3–S5 (Supplemental Material).

Results and Discussion

Evolution of PEO Structure with Temperature

The ability to detect and identify conformational changes that occur as a polymer undergoes melting and cooling transitions is of interest, in part, because the conformational structure can affect the material's mechanical properties (e.g., viscosity, heat capacity, elastic modulus).[1–3] At ambient pressure, PEO adopts an ordered structure below the crystallization temperature (T_c, 45 °C) and is highly disordered above the melting temperature (T_m, 67 °C).[4] During melting and crystallization, conformational changes that accompany the phase transitions become evident in infrared and Raman spectra, presenting as variations in band frequencies, intensities, and shapes.[15–19,47,48,58,59] Table I identifies key Raman bands for the crystalline phase based on the 7_2 helical structure. Assignments associated with various conformational structures within the temperature-dependent Raman spectra in Figures 2–3 can be understood from these assignments.

The in-situ Raman spectra in Figure 2 are from a set collected with the confocal probe volume positioned centrally within the thin (~50 μm) PEO film while the material was heated from 22 °C to 75 °C at a constant rate (1 °C /min). Below about 63 °C, PEO is in a crystalline form, and the Raman bands in Figure 2 are narrow, reflecting inter- and intra-chain ordering of oligomers within the film. As the temperature increases and approaches the melting point (67 °C), the bands begin to broaden, signaling a loss of ordering and the onset of the melting transition. Figure 2 expands the 230–1550 cm^{-1} frequency range, where the most prominent spectral changes occur. Above 63 °C, bands associated with the strong methylene and polymer backbone vibrations (Table I) show pronounced broadening and decreased intensity. The trend can be traced to conformational changes within PEO oligomers, notably rotation about the C–O bond.[47,48] Most crystalline PEO exists in a helical form arising from trans conformations of O–C and C–O bonds and gauche conformations of C–C bonds in the polymer sequence.[5,6,15–17,19,47,48,58,60] Amorphous or molten PEO, on the other hand, loses this helical structure, as most of the bonds in the backbone adopt gauche conformations.[47,48] In addition, the Raman bands in Figure 2 become more asymmetric and broader at temperatures above the melting transition due to the increased freedom of motion that leads to inhomogeneous broadening of the Raman bands.[61–65] The

Table I. Major observed Raman bands for crystalline and amorphous phases of PEO.[a]

Observed[b] (cm^{-1})	Vibrational mode assignments: Crystalline[c,d]	Vibrational mode assignments: Melt[c]	Conformation[f]
807		$r(CH_2)$	*tgg, ttt*
836		$r(CH_2)$	*ttt, ttg, gtg*
845	$r(CH_2)$a		*tgt*
860	$r\,(CH_2)$s – ν(COC)s		*tgt*
1044		$r(CH_2)$, ν(COC)	*tgg*
1063	ν(COC)s + $r(CH_2)$s		*tgt, ttt*
1092		$r(CH_2)$, ν(CO), ν(CC)	All
1126	ν(COC)s		*ttt, tgt*
1135		ν(COC)	All
1142	ν(CC) – ν(COC)a		All
1234	$\tau(CH_2)$s – $\tau(CH_2)$a		*ttt, ttg, tgt*
1244		$\tau(CH_2)$	*tgg, ggg, tgt*
1280	$\tau(CH_2)$s + $\tau(CH_2)$a		*ttt, ttg, gtg, tgt*
1286		$\tau(CH_2)$	All
1361	ω (CH_2)s + ν(CC)		*tgt*
1396	ω (CH_2)s + ν(CC)		*tgt*
1447	$\delta(CH_2)$s + $\delta(CH_2)$a		*tgg, ggg, tgt*
1471		$\delta(CH_2)$	*tgt, tgg, ggg*
1479	$\delta(CH_2)$s		*tgt*

[a]Assignments based on References.[17–19, 47]
[b]Raman band frequencies in cm^{-1} units.
[c]ν: stretch, δ: bend, ω: wag, τ: twist, r: rock.
[d]The a and s notations refer to the respective asymmetric and symmetric motions relative to the C_2-symmetry axis perpendicular to the helix axis and passing through the oxygen atom or C–C bond center. The signs (+ or –) indicate the phase relationship of the coupled coordinates.
[e]Recent work[47] suggests the bending modes at 1447 and 1479 cm^{-1} should be revised to scissoring motions.
[f]Repeating arrangement of trans (*t*) and gauche (*g*) conformations about successive O–C, C–C, and C–O bonds.

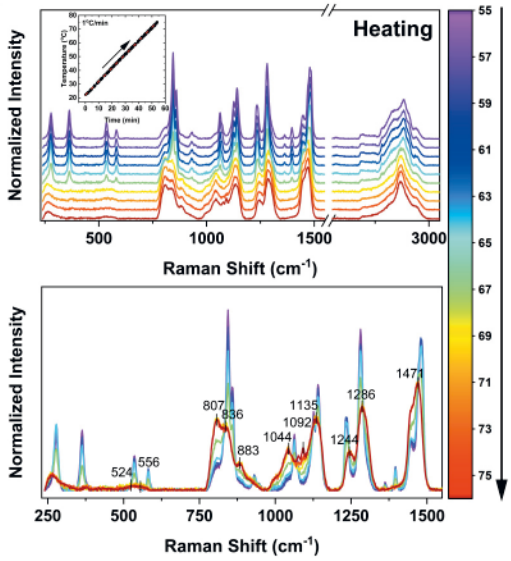

Figure 2. In situ temperature-dependent Raman spectra of PEO measured during heating at 1 °C/min. Top: Offset stacked spectra plotted between 230 and 3050 cm^{-1}. The temperature program is included in the inset. Bottom: Same spectra expanding the 230–1550 cm^{-1} region with labeled peaks. The acquisition time for each spectrum was 100 s. The ten spectra were extracted from the full dataset and are plotted with a color that corresponds to the temperature scale.

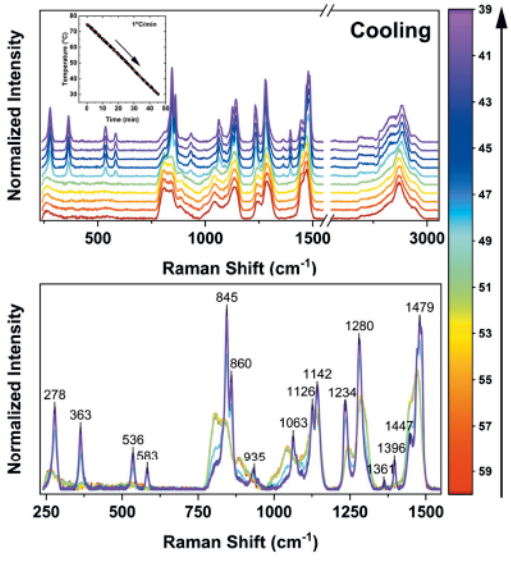

Figure 3. In situ temperature-dependent Raman spectra of PEO measured during cooling at 1 °C/min. Top: Offset stacked spectra plotted between 230 and 3050 cm^{-1}. The temperature program is included in the inset. Bottom: Same spectra expanding the 230–1550 cm^{-1} region with labeled peaks. The acquisition time for each spectrum was 100 s. The ten spectra were extracted from the full dataset and are plotted with colors corresponding to the temperature scale.

spectral differences between amorphous and crystalline PEO shown in Figure 2 have been observed in Raman measurements on bulk-phase samples. However, few of these earlier studies have reported in situ monitoring of the melting or crystallization process, as in the current work, and there have been no prior studies of thin-film samples.

The Raman spectra in Figure 3 are from a dataset that traces the cooling of a PEO thin film from 75 °C to 22 °C under the same conditions used to monitor heating of the film in Figure 2. The bands in Figure 3 are initially broad, consistent with the molten state of the material, and begin to sharpen near 50 °C, as the crystallization temperature approaches. As expected, bands associated with the methylene and polymer backbone vibrations (Table I) are most strongly affected. Comparing the spectra collected at the low temperatures (blue) in Figures 2 and 3, the reappearance of bands characteristic of a helical chain after cooling from the melt indicates that the material order/disorder phase transition under study is reversible. The structural changes that occur during PEO melting and recrystallization are considered in greater detail within the context of SMCR analysis in the next section.

Resolution and Quantification of Structural Changes in Melting and Crystallization of PEO

A common approach to follow PEO melting by its Raman scattering has been to select a mode whose frequency changes with the state of the polymer, usually the CH_2 rocking mode corresponding to the crystalline (845 cm^{-1}) and amorphous (807 cm^{-1}) states of PEO, and to use the relative scattering intensities at these two frequencies to estimate the PEO percent crystallinity.[15–19,47,48,58,59] A limitation of this approach is that these two bands are not well resolved, and band overlap can lead to quantitative inaccuracies of the results. Furthermore, unlike SMCR analysis, this approach does not extract component spectra of the evolving polymer structure. Thus, to scrutinize Raman datasets that track PEO melting and crystallization, SMCR analysis was applied to gain a more quantitative understanding of the spectral changes. Results are summarized in Figures 4 and 5, which show the pure component spectra and a plot of their respective composition vectors derived from the melting and cooling datasets, respectively.

For the melting experiment, eigenvector decomposition and matrix rotation resolved the spectra of crystalline and amorphous state polymers (Figures 4a and 4b) and the relative contributions of each component during temperature-dependent changes (Figure 4c). As the temperature increases to 75 °C, the disappearance of the crystalline form and the subsequent appearance of the amorphous form of the polymer are observed. To assess the quality of fit, the acquired data (D) and the resultant model ($\hat{D}$, the product of resolved spectral and composition component vectors) were compared. When plotted together, the two datasets cannot be

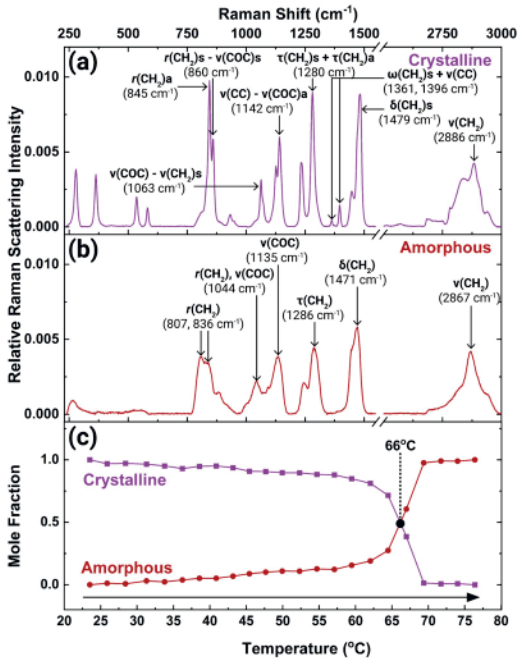

Figure 4. Pure component spectra of crystalline (a) and amorphous (b) phases derived from SMCR analysis of PEO Raman spectra recorded during melting. Temperature-dependent concentration profiles of PEO (c) show the intersection point between the two components at 66 °C. The *y*-axis reports the mole fraction of molecules in each conformational state.

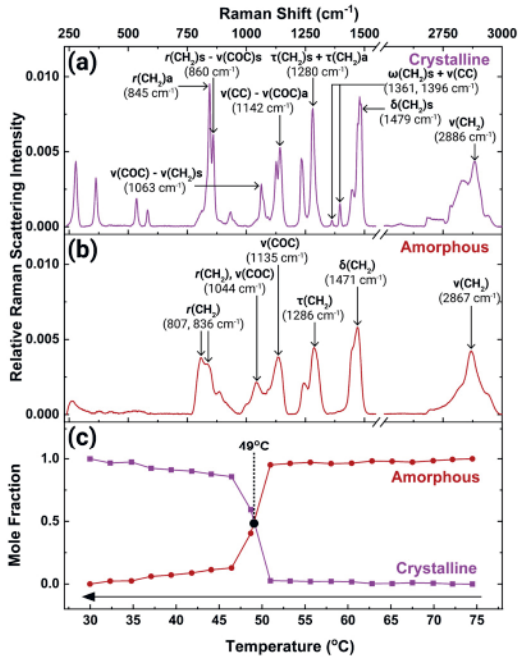

Figure 5. Pure component spectra of crystalline (a) and amorphous (b) phases derived from SMCR analysis of spectra recorded during the cooling process. Temperature-dependent concentration profiles of PEO (c) show the intersection point between the two components at 49 °C. The *y*-axis reports the mole fraction of molecules in each conformational state.

distinguished (Figure S6); the residual differences are small and random. The agreement between the two plots confirms the assumption that two distinct material structures exist within the film during the melting transition. In addition, the temperature-dependent transformation between these two structures observed in the Raman spectroscopy measurements correlates well to the changes in heat capacity with temperature that have been derived from DSC measurements.[4] The melting transition temperature determined by DSC ($T_m = 67$ °C; Figure S7) agrees within 1 °C with that determined by SMCR analysis of the Raman spectra ($T_m = 66$ °C), further supporting the self-modeling process. The expected trends in Figure 4 also indicate that the material's scattering properties and the confocal probe volume dimensions remain reasonably constant throughout the measurement, allowing for quantitative analysis of the spectral dataset. Effects of material properties on the confocal probe volume dimensions are discussed further below.

Similar to the melting transition of the PEO film, SMCR analysis was performed on the temperature-dependent data for PEO crystallization. SMCR analysis identified two components during the cooling process: a helical crystalline state and a random amorphous state, as shown in Figure 5. Upon cooling the PEO film to 30 °C, the relative contribution of the crystalline state increases, while that of the amorphous state decreases. The quality of the fit for the obtained data (D) and the product of the two-component vectors with their residuals ($\hat{D}$) is shown in Figure S8, highlighting minimal deviations of the experimental data from the model across the entire range of temperatures. The relative contributions of the two-component vectors in the SMCR results indicate a somewhat higher (4 °C) phase transition temperature for crystallization ($T_c = 49$ °C) compared to those of the DSC measurement ($T_c = 45$ °C, Figure S7). A finite-element simulation was conducted to test whether heat transfer through the coverslip to the surrounding air might account for the higher measured transition temperatures in the case of the confocal Raman measurement. The results of the simulation (presented in Figures S4 and S5, Supplemental Material) show that no thermal gradient exists across the 50 µm PEO film or between the polymer sample and the copper block where the temperature is measured. The slightly higher crystallization temperature measured for the polymer thin film may reflect compressive forces on the material, as it is sandwiched between the glass and copper block, or possibly result from the different melting temperatures accessed (120 °C in the DSC versus 75 °C in the Raman measurement) ahead of the cooling ramp.

It is notable that both the DSC measurement of a bulk sample and the Raman microscopy measurement of a thin film exhibit significant hysteresis in the crystallization of PEO. In comparing the phase transition of the melting and crystallization processes, the crystallization temperature is 22 °C lower than the melting temperature in the DSC data in Figure S7 and 17 °C lower in the thin film in Figures 4–

5. Hysteresis in the crystallization of the polymer from the melt is generally caused by slow kinetics of the polymer chain organization compared to the rate of cooling,[66,67] where the slow formation of crystalline domains from the randomly oriented aggregates allows the sample to reach a lower temperature before a fully ordered structure forms. Despite the kinetic barriers to reforming the crystalline phase apparent in the hysteresis, the structural changes associated with recrystallization from the melt appear to be reversible. Figure S9a (Supplemental Material) compares the component Raman spectra ($\hat{A}$) of the crystalline PEO film before and after melting and recrystallization. The spectra are generally in good agreement, but with slight differences likely traceable to sample history. The crystalline form derived from the melting experiment reflects a sample that has been at ambient temperature for an extended period, while the crystalline form vector derived from the cooling experiment is for a sample that has been below the transition temperature for less than 15 min. The slow rearrangement (and ordering) of polymer chains from a viscous sample, manifested in the hysteresis of the transition temperatures, could explain the slight differences in the Figure S9a spectra. The difference may show that the crystalline state of PEO that forms immediately upon cooling below the transition temperature is not identical to one that has been below the transition temperature for much longer period of time, where further ordering of the polymer chains could occur. Nevertheless, the response in Figure S9a indicates the stability of the PEO through melting and cooling, the reversibility of the phase transition, and the recovery of a comparable structure upon recrystallization. A related comparison for the amorphous phase, where agreement between the two spectral vectors is much closer, is shown in Figure S9b.

Detailed Analysis of the Structural Changes upon Melting and Crystallization of PEO

In addition to revealing the phase transition behavior of polymer thin films, in situ confocal Raman microscopy combined with SMCR analysis of the data produces resolved component spectra that provide insights into the structural changes associated with melting and recrystallization. The following paragraphs consider several spectral regions that are informative of changes in the structure of the polymer.

C–O–C Bending Region (230–600 cm^{-1}). The frequency region below 600 cm^{-1} is influenced by conformational changes due to rotations about C–O bonds.[15,16,18,19] Raman bands near 278, 363, 536, and 583 cm^{-1}, correspond mainly to C–C–O and C–O–C bending vibrations. The bands become sharper and increase in intensity as the PEO polymer cools from 75 °C to 25 °C. In particular, the sharp bands at 536 and 583 cm^{-1} in spectra of the crystalline solid and the weak, broad features at 524 and 556 cm^{-1} in spectra of the molten material exhibit considerable differences associated with changes in the C–O bond configuration. The 536 and 583 cm^{-1} bands are linked to the trans–trans conformation of successive O–C and C–O bonds in the crystalline solid, while the 524 and 556 cm^{-1} features are associated with a mixture of trans–gauche and gauche–gauche conformations of the successive O–C and C–O bonds in the melt phase.[15]

CH_2 Rocking and C–O–C Stretching Regions (800–1150 cm^{-1}). The methylene rocking and C–O–C stretching regions between 800 and 1150 cm^{-1} in Raman spectra of PEO prominently display structural changes during phase transitions. As the molten PEO polymer film is cooled from 75 °C to 30 °C, the broad bands associated with CH_2 rocking vibrations near 807, 836, and 1044 cm^{-1} sharpen and shift to 845, 860, and 1063 cm^{-1}, respectively. The CH_2 rocking bands at 807 and 845 cm^{-1} are of particular interest. The feature at 807 cm^{-1} is a characteristic of the gauche O–C and C–O conformation in the amorphous state and decreases in intensity as the PEO polymer crystallizes. Meanwhile, sharpening of the band at 845 cm^{-1} is associated with the development of the gauche configuration of the C–C bond and the trans configuration of the O–C and C–O bonds, consistent with a helical structure with a repeating arrangement of trans–gauche–trans configuration in O–C, C–C, and C–O bonds, respectively.[47,58] Additionally, the transformation of the broad Raman band at 1044 cm^{-1} in the molten state to a sharp feature at 1063 cm^{-1} in the crystalline state further indicates conformational ordering within the polymer.[15,47] These two Raman bands at 1044 and 1063 cm^{-1} are attributed to coupled CH_2 rocking and C–O–C stretching vibrational modes (Table I).[15–19,58,60,68] These spectral changes during the cooling process confirm the rotation of the O–C and C–O bonds from a gauche configuration in the molten state to the trans configuration in the crystalline state.[15,47]

CH_2 Twisting Region (1150–1300 cm^{-1}). Another interesting spectral region related to methylene group motions involves the CH_2 twisting modes. During cooling of the PEO polymer, the broad Raman bands characteristic of CH_2 twisting at 1244 and 1286 cm^{-1} sharpen and evolve into more complicated C–C group modes of the crystalline polymer (Table I), which has corresponding peaks at 1234 and 1280 cm^{-1}. Despite several possible contributing conformations, the broad Raman band at 1286 cm^{-1} for molten PEO is generally attributed to trans conformations of the O–C, C–C, and C–O bonds.[15,16,18,19] The Raman band observed at 1234 cm^{-1} for crystalline PEO is associated with the gauche configuration of the C–C bond in the 7_2 helical structure.[60,68]

CH_2 Wagging and C–C Stretching Region (1300–1400 cm^{-1}). In the 1300–1400 cm^{-1} frequency region, sharp increases in Raman band intensities at 1361 and 1396 cm^{-1} are observed as the PEO polymer cools. Both the 1361 and 1396 cm^{-1} bands have been assigned to combination modes associated with symmetric

CH_2 wagging and C–C stretching fundamentals.[15–19,47,48,58,59] The Raman band at 1361 cm^{-1} is attributed to the C–C gauche configuration of the helical crystalline state.[18]

CH_2 Bending Region (1400–1500 cm^{-1}). The 1400–1500 cm^{-1} frequency region contains Raman bands associated with CH_2 bending modes. Specifically, the broad Raman feature near 1471 cm^{-1} in molten PEO sharpens and splits into two bands (1447 and 1479 cm^{-1}) attributed to CH_2 bending[5,15,16,60] (or CH_2 scissoring[18,19,47]) modes in the crystalline state.

CH_2 Stretching Region (2800–3000 cm^{-1}). While the CH_2 stretching region is challenging to interpret due to Fermi resonance interactions, studies indicate that changes in this region are highly sensitive to conformational ordering and disordering.[47,61,69] In the molten state, a broad Raman band is observed at 2867 cm^{-1}. This CH_2 stretching band shifts to 2886 cm^{-1} and increases in intensity, forming a broad Raman band at 2939 cm^{-1} upon cooling of the PEO polymer. The two prominent vibrational frequencies at 2886 cm^{-1} and 2939 cm^{-1} in the crystalline state are characteristic of symmetric CH_2 stretching and anti-symmetric CH_2 stretching modes, respectively. Recent studies suggested that these two bands at 2886 cm^{-1} and 2939 cm^{-1} provide insights into the degree of inter-chain interactions within PEO. The Raman band intensity ratio of the symmetric CH_2 stretching band (2886 cm^{-1}) to the anti-symmetric CH_2 stretching band (2939 cm^{-1}) decreases during the melting process, suggesting increased disruption of inter-chain coupling in the molten state compared to the crystalline state.

Confocal Depth Resolution and Detection of Thinner PEO Films

The demonstrated methodology has the potential to be extended to thinner polymer films. To explore the limits, the strategy to estimate axial spatial resolution in confocal Raman microscopy depth profiling was applied to understand the relationship between the confocal probe volume dimensions and the thickness of the materials under study.[30,32,34,70] Given its atomic-scale thickness, SLG was depth profiled to estimate the instrument response function (IRF) of the confocal Raman microscopy setup employed. As shown in Figure S10 (Supplemental Material), the scattering intensity of the graphene 2D vibration at 2636 cm^{-1} plotted as the confocal probe volume was scanned through the monolayer graphene film fits a Lorentzian function with a full width at half-maximum (FWHM) of 4.0 μm. The result closely matches measurements reported by Sacco and coworkers[32] for a similar air objective. The response shows that the confocal probe volume axial dimension (10.1 μm at 63% detection efficiency or $6 \times 4.0\ \mu m = 24\ \mu m$ at 90% detection efficiency)[29] is smaller than the thickness of the 50 μm film used in the study of PEO melting transitions. However, as film thickness decreases, care is needed to maintain sample alignment within the confocal probe volume for optimum sensitivity.

To test the capability to measure thinner polymer films, a study was extended to a ~2 μm thickness PEO film. As shown in Figure S11 (Supplemental Material), a Raman spectrum of the film exhibits a signal-to-noise ratio (S/N) > 30 for the most intense bands. To assess the depth resolution, the scattering intensity of the CH_2 twisting band at 1280 cm^{-1} was plotted as the confocal probe volume position was stepped through the sample (Figure S11, Supplemental Material). Included in the plot is the result of calculating the convolution of a Lorentzian IRF with a 2 μm rectangular function representing the PEO film on the glass substrate. The Lorentzian function in this fit has a FWHM of 5.9 μm. Although somewhat greater than the 4.0 μm FWHM measured with SLG, the broadened response reflects the effects of refraction and spherical aberration.[28,29,36,38] Both are pronounced when measuring within a polymer using an air objective due to the large refractive index mismatch as radiation propagates between air ($n = 1.0$) and the polymer phase ($n \approx 1.4$). Nevertheless, it is significant that the optical distortions are not great in measurements on the ~2 μm PEO film and will be reduced as the sample thickness becomes smaller. The results show that a confocal Raman microscope equipped with an air objective can be extended to probe within 2 μm and potentially thinner polymer films. Furthermore, for materials supported on a reflective substrate, as shown in Figure 1, there is potential to gain heightened sensitivity by taking advantage of electric field enhancements in the focal region.[71] This exploration of thin (~2 μm) PEO films opens possibilities for monitoring structural changes and transition temperatures of other thin-film supported polymers, including films containing ultrathin confined layers,[72] during melting and crystallization.

Conclusion

Confocal Raman microscopy was applied to probe within a 50 μm thickness PEO film, providing insights into the molecular-level structural changes that occur as the thin film progressed through an order-disorder phase transition during heating and cooling. SMCR analysis of the spectral datasets identified two pure component spectra. One spectral vector had features in common with the 7_2 helical structure of crystalline PEO and the other traced to the amorphous phase of molten PEO. The SMCR analysis effectively addressed the challenge of resolving spectra of the ordered and disordered states of the polymer without prior knowledge of Raman band assignments or the need to fit overlapping spectral peaks. Furthermore, the concentration vectors derived from the SMCR analysis of the Raman data enabled (i) the relative contributions of the two phases to be followed quantitatively as a function of temperature and (ii) the phase transition temperatures for PEO melting and crystallization to be estimated. The measurement

approach opens opportunities for monitoring molecular-level changes associated with thermal transitions within supported polymer films as thin as 2 µm, samples that are not easily adapted to study by conventional thermal analysis techniques. Confocal Raman microscopy coupled with SMCR analysis is a robust methodology that can support efforts to gain fundamental insights into molecular mechanisms in the thermal processing of thin-film polymers.

Acknowledgments

We gratefully acknowledge financial support from the U.S. National Science Foundation (NSF) through grants CBET-1922956 (CK), CBET-1921075 (SDM), and the NSF Graduate Research Fellowship under Grant No. 1747505 (ADP). The construction of the confocal Raman microscope was supported by the U.S. Department of Energy under award DE-FG03-93ER14333. The SEM images were collected with the support of the MRSEC Program of NSF under Award No. DMR-1121252 and the University of Utah USTAR shared facilities. DSC measurements were performed at the University of Utah's Materials Characterization Lab. Finally, we thank machinist Dusty Layton (UU) for assistance with cell design and fabrication and a reviewer for their guidance concerning polymer cooling transitions.

Declaration of Conflicting Interests

The authors declared no potential conflicts of interest with respect to the research, authorship, and/or publication of this article.

Funding

The authors disclose receipt of the following financial support for the research, authorship, and/or publication of this article: This work was supported by the NSF Division of Graduate Education, DOE Basic Energy Sciences, NSF Division of Chemical, Bioengineering, Environmental, and Transport Systems, NSF Division of Materials Research (grant numbers: DGE-1747505, DE-FG03-93ER14333, CBET-1921075 , CBET-1922956 , DMR-1121252).

ORCID iDs

Miharu Koh https://orcid.org/0000-0001-9677-2504
Jay P. Kitt https://orcid.org/0000-0002-1469-3659
Andrew D. Pendergast https://orcid.org/0000-0003-3311-1260
Joel M. Harris https://orcid.org/0000-0002-7081-8188
Carol Korzeniewski https://orcid.org/0000-0003-3672-0731

Supplemental Material

All supplemental material mentioned in the text is available in the online version of the journal.

References

1. D.M. Bigg. "Mechanical Property Enhancement of Semicrystalline Polymers: A Review". Polym. Eng. Sci. 1988. 28(13): 830-841.
2. D.C. Bassett. "Polymer Spherulites: A Modern Assessment". J. Macromol. Sci., Part B: Phys. 2003. 42(2): 227-256.
3. T.D. Horn, D. Heidrich, H. Wulf, M. Gehde, J. Ihlemann. "Multiscale Simulation of Semi-Crystalline Polymers to Predict Mechanical Properties". Polymers. 2021. 13(19): 3233.
4. J. Jin, M. Song, F. Pan. "A DSC Study of Effect of Carbon Nanotubes on Crystallisation Behaviour of Poly(Ethylene Oxide)". Thermochim. Acta. 2007. 456(1): 25-31.
5. H. Tadokoro, Y. Chatani, T. Yoshihara, S. Tahara, S. Murahashi. "Structural Studies on Polyethers, $[-(CH_2)_m-O-]_n$. II. Molecular Structure of Polyethylene Oxide". Makromol. Chem. 1964. 73(1): 109-127.
6. Y. Takahashi, I. Sumita, H. Tadokoro. "Structural Studies of Polyethers. IX. Planar Zigzag Modification of Poly(Ethylene Oxide)". J. Polym. Sci., Part B: Polym. Phys. 1973. 11(11): 2113-2122.
7. Y. Takahashi, H. Tadokoro. "Structural Studies of Polyethers, (–(CH_2)m–O–)n. X. Crystal Structure of Poly(Ethylene Oxide)". Macromolecules. 1973. 6(5): 672-675.
8. G.M. Kelly, J.F. Elman, Z. Jiang, J. Strazalka, J.N.L. Albert. "Thermal Transitions in Semi-Crystalline Polymer Thin Films Studied via Spectral Reflectance". Polymer. 2018. 143: 336-342. 10.1016/j.polymer.2018.04.017
9. J. Kugler, E.W. Fischer, M. Peuscher, C.D. Eisenbach. "Small Angle Neutron Scattering Studies of Poly(Ethylene Oxide) in the Melt". Makromol. Chem. 1983. 184(11): 2325-2334.
10. G. Allen, T. Tanaka. "A Small-Angle Neutron Scattering Study on Poly(Ethylene Oxide) Crystals". Polymer. 1978. 19(3): 271-276.
11. A. Johansson, J. Tegenfeldt. "NMR Study of Crystalline and Amorphous Poly(Ethylene Oxide)". Macromolecules. 1992. 25 (18): 4712-4715.
12. T.M. Connor, K.A. McLauchlan. "High Resolution Nuclear Resonance Studies of the Chain Conformation of Polyethylene Oxide". J. Phys. Chem. 1965. 69(6): 1888-1893.
13. Y. Hiejima, K. Takeda, K. Nitta. "Investigation of the Molecular Mechanisms of Melting and Crystallization of Isotactic Polypropylene by In Situ Raman Spectroscopy". Macromolecules. 2017. 50(15): 5867-5876.
14. C. Minogianni, K.G. Gatos, C. Galiotis. "Estimation of Crystallinity in Isotropic Isotactic Polypropylene with Raman Spectroscopy". Appl. Spectrosc. 2005. 59(9): 1141-1147.
15. J.L. Koenig, A.C. Angood. "Raman Spectra of Poly(Ethylene Glycols) in Solution". J. Polym. Sci., Part B: Polym. Phys. 1970. 8(10): 1787-1796.
16. J. Maxfield, I.W. Shepherd. "Conformation of Poly(Ethylene Oxide) in the Solid State, Melt and Solution Measured by Raman Scattering". Polymer. 1975. 16(7): 505-509.
17. T. Yoshihara, H. Tadokoro, S. Murahashi. "Normal Vibrations of the Polymer Molecules of Helical Conformation. IV. Polyethylene Oxide and Polyethylene-d_4 Oxide". J. Chem. Phys. 1964. 41(9): 2902-2911.
18. H. Matsuura, K. Fukuhara. "Vibrational Spectroscopic Studies of Conformation of Poly(Oxyethylene). II. Conformation–Spectrum Correlations". J. Polym. Sci., Part B: Polym. Phys. 1986. 24(7): 1383-1400.
19. K. Chrissopoulou, K.S. Andrikopoulos, S. Fotiadou, S. Bollas, et al. "Crystallinity and Chain Conformation in PEO/Layered Silicate Nanocomposites". Macromolecules. 2011. 44(24): 9710-9722.
20. R.V. Chimenti, J.T. Carriere, D.M. D'Ascoli, J.D. Engelhardt, et al. "Toward a Practical Method for Measuring Glass Transition in

Polymers with Low-Frequency Raman Spectroscopy". Appl. Phys. Lett. 2023. 122(26): 264101.
21. Meng H., X. Yu, H. Feng, Z. Xue, N. Yang. "Superior Thermal Conductivity of Poly(Ethylene Oxide) for Solid-State Electrolytes: A Molecular Dynamics Study". Int. J. Heat Mass Transfer. 2019. 137: 1241-1246. 10.1016/j.ijheatmasstransfer.2019.04.021
22. X. Li, X. Yu, Y. Han. "Polymer Thin Films for Antireflection Coatings". J. Mater. Chem. C. 2013. 1(12): 2266-2285.
23. K.L. Chopra, P.D. Paulson, V. Dutta. "Thin-Film Solar Cells: An Overview". Prog. Photovolt: Res. Appl. 2004. 12(2–3): 69-92.
24. G. Li, R. Zhu, Y. Yang. "Polymer Solar Cells". Nat. Photonics. 2012. 6 (3): 153-161. 10.1038/nphoton.2012.11
25. Y. Degani, A. Heller. "Electrical Communication Between Redox Centers of Glucose Oxidase and Electrodes via Electrostatically and Covalently Bound Redox Polymers". J. Am. Chem. Soc. 1989. 111(6): 2357-2358.
26. R.D. Milton, D.P. Hickey, S. Abdellaoui, K. Lim, et al. "Rational Design of Quinones for High Power Density Biofuel Cells". Chem. Sci. 2015. 6(8): 4867-4875.
27. D.P. Hickey, R.C. Reid, R.D. Milton, S.D. Minteer. "A Self-Powered Amperometric Lactate Biosensor Based on Lactate Oxidase Immobilized in Dimethylferrocene-Modified LPEI". Biosens. Bioelectron. 2016. 77: 26-31. 10.1016/j.bios.2015.09.013
28. N.J. Everall. "Confocal Raman Microscopy: Performance, Pitfalls, and Best Practice". Appl. Spectrosc. 2009. 63(9): 245A-262A.
29. N.J. Everall. "Confocal Raman Microscopy: Common Errors and Artefacts". Analyst. 2010. 135(10): 2512-2522.
30. T.E. Bridges, M.P. Houlne, J.M. Harris. "Spatially Resolved Analysis of Small Particles by Confocal Raman Microscopy: Depth Profiling and Optical Trapping". Anal. Chem. 2004. 76 (3): 576-584.
31. J. Xu, M. Koh, S.D. Minteer, C. Korzeniewski. "In Situ Confocal Raman Microscopy of Redox Polymer Films on Bulk Electrode Supports". ACS Meas. Sci. Au. 2023. 3(2): 127-133.
32. A. Sacco, C. Portesi, A.M. Giovannozzi, A.M. Rossi. "Graphene Edge Method for Three-Dimensional Probing of Raman Microscopes Focal Volumes". J. Raman Spectrosc. 2021. 52(10): 1671-1684.
33. T.E. Bridges, R.H. Uibel, J.M. Harris. "Measuring Diffusion of Molecules into Individual Polymer Particles by Confocal Raman Microscopy". Anal. Chem. 2006. 78(7): 2121-2129.
34. C. Korzeniewski, J.P. Kitt, S. Bukola, S.E. Creager, et al. "Single Layer Graphene for Estimation of Axial Spatial Resolution in Confocal Raman Microscopy Depth Profiling". Anal. Chem. 2019. 91(1): 1049-1055.
35. J.P. Kitt, J.M. Harris. "Confocal Raman Microscopy for In Situ Measurement of Octanol–Water Partitioning Within Pores of Individual C_{18}-Functionalized Chromatographic Particles". Anal. Chem. 2015. 87(10): 5340-5347.
36. J.P. Kitt, D.A. Bryce, J.M. Harris. "Spatial Filtering of a Diode Laser Beam for Confocal Raman Microscopy". Appl. Spectrosc. 2015. 69(4): 513-517.
37. N.J. Everall. "Modeling and Measuring the Effect of Refraction on the Depth Resolution of Confocal Raman Microscopy". Appl. Spectrosc. 2000. 54(6): 733-782. doi:10.1366/0003702001950382
38. R. Tabaksblat, R.J. Meier, B.J. Kip. "Confocal Raman Microspectroscopy: Theory and Application to Thin Polymer Samples". Appl. Spectrosc. 1992. 46(1): 60-68.
39. J.J. Schaefer, A.C. Crawford, M.D. Porter, J.M. Harris. "Confocal Raman Microscopy for Investigating Synthesis and Characterization of Individual Optically Trapped Vinyl-Polymerized Surfactant Particles". Appl. Spectrosc. 2014. 68(6): 633-641.
40. J.J. Schaefer, C.B. Fox, J.M. Harris. "Confocal Raman Microscopy for Monitoring the Membrane Polymerization and Thermochromism of Individual, Optically Trapped Diacetylenic Phospholipid Vesicles". J. Raman Spectrosc. 2012. 43(3): 351-359.
41. C.B. Fox, R.A. Horton, J.M. Harris. "Detection of Drug-Membrane Interactions in Individual Phospholipid Vesicles by Confocal Raman Microscopy". Anal. Chem. 2008. 78(14): 4918-4924. doi:10.1021/ac0605290
42. C.A. Froud, I.P. Hayward, J. Laven. "Advances in the Raman Depth Profiling of Polymer Laminates". Appl. Spectrosc. 2003. 57(12): 1468-1474.
43. A. Apicella, B. Cappello, M.A. Del Nobile, M.I. La Rotonda, et al. "Poly(Ethylene Oxide) (PEO) and Different Molecular Weight PEO Blends Monolithic Devices for Drug Release". Biomaterials. 1993. 14(2): 83-90.
44. E. Quartarone, P. Mustarelli, A. Magistris. "PEO-Based Composite Polymer Electrolytes". Solid State Ionics. 1998. 110(1–2): 1-14.
45. C.A.P. Quinn, R.E. Connor, A. Heller. "Biocompatible, Glucose-Permeable Hydrogel for In Situ Coating of Implantable Biosensors". Biomaterials. 1997. 18(24): 1665-1670.
46. H. Matsuura, T. Miyazawa. "Vibrational Analysis of Molten Poly (Ethylene Glycol)". J. Polym. Sci., Part B: Polym. Phys. 1969. 7(10): 1735-1744.
47. A.Z. Samuel, S. Umapathy. "Energy Funneling and Macromolecular Conformational Dynamics: A 2D Raman Correlation Study of PEG Melting". Polym. J. 2014. 46(6): 330-336. 10.1038/pj.2014.10
48. E.A. Sagitova, K.A. Prokhorov, G.Y. Nikolaeva, A.V. Baimova, et al. "Raman Analysis of Polyethylene Glycols and Polyethylene Oxides". J. Phys.: Conf. Ser. 2018. 999: 012002. 10.1088/1742-6596/999/1/012002
49. W.H. Lawton, E.A. Sylvestre. "Self-Modeling Curve Resolution". Technometrics. 1971. 13(3): 617-633.
50. E.R. Malinowski. Factor Analysis in Chemistry. New York: John Wiley and Sons, 1991.
51. E.R. Malinowski, R.A. Cox, U.L. Haldna. "Factor Analysis for Isolation of the Raman Spectra of Aqueous Sulfuric Acid Components". Anal. Chem. 1984. 56(4): 778-781.
52. K.P.J. Williams, G.D. Pitt, D.N. Batchelder, B.J. Kip. "Confocal Raman Microspectroscopy Using a Stigmatic Spectrograph and CCD Detector". Appl. Spectrosc. 1994. 48(2): 232-235.
53. D.E. Koppel, D. Axelrod, J. Schlessinger, E.L. Elson, W.W. Webb. "Dynamics of Fluorescence Marker Concentration as a Probe of Mobility". Biophys. J. 1976. 16(11): 1315-1329.
54. C.B. Fox, R.H. Uibel, J.M. Harris. "Detecting Phase Transitions in Phosphatidylcholine Vesicles by Raman Microscopy and Self-Modeling Curve Resolution". J. Phys. Chem. B. 2007. 111 (39): 11428-11436.
55. J.P. Kitt, J.M. Harris. "Confocal Raman Microscopy of Hybrid-Supported Phospholipid Bilayers Within Individual C_{18}-Functionalized Chromatographic Particles". Langmuir. 2016. 32(35): 9033-9044.
56. J.P. Kitt, D.A. Bryce, J.M. Harris. "Calorimetry-Derived Composition Vectors to Resolve Component Raman Spectra

in Phospholipid Phase Transitions". Appl. Spectrosc. 2016. 70(7): 1165-1175.
57. N.N. Brandt, O.O. Brovko, A.Y. Chikishev, O.D. Paraschuk. "Optimization of the Rolling-Circle Filter for Raman Background Subtraction". Appl. Spectrosc. 2006. 60(3): 288-293.
58. T. Miyazawa, K. Fukushima, Y. Ideguchi. "Molecular Vibrations and Structure of High Polymers. III. Polarized Infrared Spectra, Normal Vibrations, and Helical Conformation of Polyethylene Glycol". J. Chem. Phys. 1962. 37(12): 2764-2776.
59. V.V. Kuzmin, V.S. Novikov, L.Y. Ustynyuk, K.A. Prokhorov, et al. "Raman Spectra of Polyethylene Glycols: Comparative Experimental and DFT Study". J. Mol. Struct. 2020. 1217: 128331.
60. Y. Ding, J.F. Rabolt, Y. Chen, K.L. Olson, G.L. Baker. "Studies of Chain Conformation in Triblock Oligomers and Microblock Copolymers of Ethylene and Ethylene Oxide". Macromolecules. 2002. 35(10): 3914-3920.
61. C.J. Orendorff, M.W. Ducey Jr., J.E. Pemberton. "Quantitative Correlation of Raman Spectral Indicators in Determining Conformational Order in Alkyl Chains". J. Phys. Chem. A. 2002. 106(30): 6991-6998.
62. S.L. Wunder. "Raman Spectroscopic Study of the High-Pressure Phase of Polyethylene". Macromolecules. 1981. 14(4): 1024-1030.
63. S.L. Wunder, M.I. Bell, G. Zerbi. "Band Broadening of CH_2 Vibrations in the Raman Spectra of Polymethylene Chains". J. Chem. Phys. 1986. 85(7): 3827-3839.
64. R.G. Snyder, S.L. Hsu, S. Krimm. "Vibrational Spectra in the C–H Stretching Region and the Structure of the Polymethylene Chain". Spectrochim. Acta, Part A. 1978. 34(4): 395-406.
65. R.G. Snyder, H.L. Strauss, C.A. Elliger. "C–H Stretching Modes and the Structure of N-Alkyl Chains. 1. Long, Disordered Chains". J. Phys. Chem. 1982. 86(26): 5145-5150.
66. M.R. Berber, H. Mori, I.H. Hafez, K. Minagawa, et al. "Unusually Large Hysteresis of Temperature-Responsive Poly(N-Ethyl-2-Propionamidoacrylamide) Studied by Microcalorimetry and FT-IR". J. Phys. Chem. B. 2010. 114(23): 7784-7790.
67. J. Noel, Y. Jannot, C. M´etivier, N.R. Sgreva. "Thermal Characterization of Polyethylene Glycol 600 in Liquid and Solid Phase and Across the Phase Transition". Thermochim. Acta. 2022. 716: 179326. 10.1016/j.tca.2022.179326
68. M. Richard-Lacroix, C. Pellerin. "Raman Spectroscopy of Individual Poly(Ethylene Oxide) Electrospun Fibers: Effect of the Collector on Molecular Orientation". Vib. Spectrosc. 2017. 91: 92-98. 10.1016/j.vibspec.2016.09.002
69. I.R. Hill, I.W. Levin. "Vibrational Spectra and Carbon–Hydrogen Stretching Mode Assignments for a Series of N-Alkyl Carboxylic Acids". J. Chem. Phys. 1979. 70(2): 842-851.
70. C.J. De Grauw, N.M. Sijtsema, C. Otto, J. Greve. "Axial Resolution of Confocal Raman Microscopes: Gaussian Beam Theory and Practice". J. Microsc. 1997. 188(3): 273-279.
71. M.Y. Wu, D.X. Liang, L. Ling, W. Li, Y.Q. Li. "Stable Optical Trapping and Sensitive Characterization of Nanostructures Using Standing-Wave Raman Tweezers". Sci. Rep. 2017. 7: 42930. 10.1038/srep42930
72. H. Wang, J.K. Keum, A. Hiltner, E. Baer. "Crystallization Kinetics of Poly(Ethylene Oxide) in Confined Nanolayers". Macromolecules. 2010. 43(7): 3359-3364.